Aalborg University

DENMARK

Impact of Circular Current Limiters on Transient Stability of Grid-Forming Converters

Fan, Bo; Wang, Xiongfei

Impact of Circular Current Limiters on Transient Stability of Grid-Forming Converters

Bo Fan, Xiongfei Wang*

AAU Energy, Aalborg University, Aalborg, Denmark

*E-mail: xwa@energy.aau.dk

Abstract—**This study investigates the transient stability of a virtual-admittance-controlled grid-forming (GFM) converter with a circular current limiter. Firstly, to facilitate the transient stability analysis, the inner control loops along with the circular current limiter are represented as a voltage source behind adaptive virtual impedance. Next, a time-rescaling technique is utilized to simplify the closed-loop system dynamics. It is found that transient stability is only affected by the "relative speed" defined as the ratio between the voltage magnitude control gain and the power one. Based on the simplified system model, the phase plain analysis is applied to evaluate the transient stability of the GFM converter. The results reveal that transient stability can be jeopardized when the circular current limiter is applied, while reacquired by increasing the relative speed. Finally, simulation and experimental tests are conducted to verify these findings.**

Keywords—*Current limiter, grid-forming converter, transient stability, virtual admittance control.*

I. Introduction

To integrate increasing converter-interfaced generators into power grids, grid-forming (GFM) control is recognized as an effective solution [1]. The GFM converters can directly regulate their output voltages and frequencies, which improves not only the power grid stability but also its resilience [2].

The current outputs of GFM converters are determined by electrical network conditions since they are controlled as voltage sources behind impedance [2]. Due to the limited overcurrent capability of semiconductor devices, current-limiting strategies are usually required to protect the converters against disturbances or faults [3]. Usually, two types of current-limiting strategies are used. One is virtual impedance [4], [5], and the other one is current limiters [6]–[8].

With these methods, the ability of GFM converters to maintain synchronism with a power system, i.e., their transient stability [9], needs to be evaluated. Recently, this problem is investigated in [5]–[7] with ignored inner control loop dynamics. But these results are not applicable for circular current limiters [8], [10] whose outputs are coupled with the inner voltage control loops such as virtual admittance control [10]. Therefore, this study aims to investigate the impact of
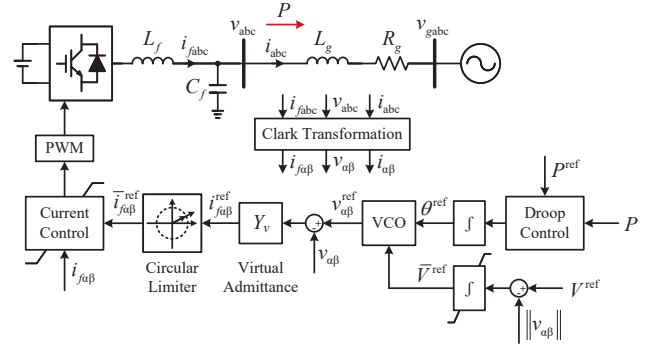
Fig. 1. A virtual-admittance-controlled GFM converter with the circular current limiter.

circular current limiters on the transient stability of a virtual-admittance-controlled GFM converter. The contributions are listed as follows:

1) An equivalent circuit model is established for the transient stability analysis of GFM converters. It is revealed that the inner control loops with the circular current limiter can be modeled as a voltage source behind adaptive virtual impedance.

2) A time-rescaling technique is used to simplify the closed-loop system dynamics, which shows that the transient stability is dependent on the "relative speed" between the voltage magnitude control loop and the power one.

3) Based on the phase plane analysis, it shows that transient stability can be jeopardized when the circular current limiter is used, while reacquired by increasing the defined relative speed.

Finally, these findings are validated by simulation and experimental tests.

Notation: For a physical variable x, $x_{\text{abc}} \in \mathbb{R}^3$ and $x_{\alpha\beta} \in \mathbb{C}$ denote x in the natural reference frame (abc-frame) and the stationary reference frame ($\alpha\beta$-frame), respectively. Further, for a complex variable $y \in \mathbb{C}$, $y^* \in \mathbb{C}$ and $\|y\| \in \mathbb{R}$ represent the conjugate and modulus of y, respectively. $\text{j} \in \mathbb{I}$ represents the unit imaginary number.

II. GFM Converters With Circular Limiters

A. System Description

The overall system of the considered grid-connected GFM converter is illustrated in Fig. 1. L_f and C_f are the *LC*-filter
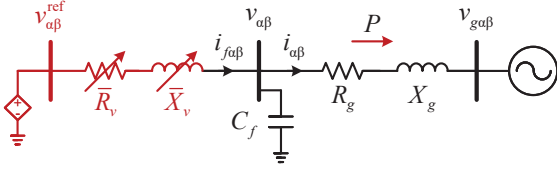
Fig. 2. Proposed equivalent circuit model.

inductance and capacitance. L_g and R_g are the grid impedance.

For the outer control loops, power control and voltage magnitude control are used to regulate the active power output and the capacitor voltage, respectively. For the inner control loops, a virtual admittance is applied to generate the converter-side current reference [10]. To prevent the converter from over-current, a circular current limiter is utilized to restrict the current reference that is further achieved by a quasi-proportional-resonant current controller [11]. i_{fabc} and i_{abc} are the converter-side and grid-side currents, respectively. v_{gabc} and v_{abc} are the grid and capacitor voltages, respectively.

B. Control Structure

The power control is expressed as

$$\dot{\theta}^{\text{ref}} = \omega_g + K_P^P (P^{\text{ref}} - P) \tag{1}$$

where θ^{ref} is the phase angle of the voltage reference $v_{\alpha\beta}$; K_P^P is the power control gain; P^{ref} is the active power reference; $P = \text{Re}\{v_{\alpha\beta} i_{\alpha\beta}^*\}$ is the active power output of the converter.

The voltage magnitude control loop is represented as

$$\dot{V}^{\text{ref}} = K_P^V (V^{\text{ref}} - \|v_{\alpha\beta}\|) \tag{2}$$

where $\bar{V}^{\text{ref}}$ is the magnitude of $v_{\alpha\beta}^{\text{ref}}$; K_P^V is the constant voltage control gain; V^{ref} is the capacitor voltage magnitude reference.

Once the circular current limiter is triggered, the capacitor voltage $\|v_{\alpha\beta}\|$ cannot track it reference V^{ref} anymore. To avoid the windup of the voltage magnitude control integrator, its input is set as zero, i.e., $K_P^V = 0$, during the current-limiting period.

The expression of the circular current limiter is given by

$$\bar{i}_{f\alpha\beta}^{\text{ref}} = \sigma i_{f\alpha\beta}^{\text{ref}}, \quad \sigma \triangleq \min\left\{1, I_M / \|i_{f\alpha\beta}^{\text{ref}}\|\right\} \tag{3}$$

where $i_{f\alpha\beta}^{\text{ref}} = Y_v(v_{\alpha\beta}^{\text{ref}} - v_{\alpha\beta})$ is the original current reference with $Y_v = 1/(sL_v + R_v)$ being the virtual admittance; $\bar{i}_{f\alpha\beta}^{\text{ref}}$ is the saturated current reference; and I_M is the maximum allowable converter-side current magnitude.

In this study, the following commonly used assumptions in transient stability analysis [5]–[7] are introduced: 1) ignore the current control loop dynamics, i.e., $i_{f\alpha\beta} = \bar{i}_{f\alpha\beta}^{\text{ref}}$; 2) ignore the capacitor's and inductors' dynamics.

III. DYNAMIC REPRESENTATION OF GFM CONVERTERS

A. Equivalent Circuit Model

To facilitate the transient stability analysis, this section introduces an equivalent circuit model of the considered GFM converter shown in Fig. 1.

Based on the aforementioned assumptions, the virtual admittance becomes $Y_v = 1/(jX_v + R_v)$ with $X_v = \omega_g L_v$. Further, with the assumption $i_{f\alpha\beta} = \bar{i}_{f\alpha\beta}^{\text{ref}}$ and (3), one has

$$i_{f\alpha\beta} = \sigma Y_v(v_{\alpha\beta}^{\text{ref}} - v_{\alpha\beta}) \Rightarrow (\bar{R}_v + j\bar{X}_v)i_{f\alpha\beta} = v_{\alpha\beta}^{\text{ref}} - v_{\alpha\beta} \tag{4}$$

where $\bar{R}_v = R_v/\sigma$ and $\bar{X}_v = X_v/\sigma$. Hence, the inner control loops with the circular current limiter can be represented as a voltage source behind adaptive virtual impedance $\bar{R}_v + j\bar{X}_v$ as shown in Fig. 2.

Notice that according to (3), if the circular current limiter is not triggered, i.e., $\sigma = 1$, then one has $\bar{R}_v = R_v$ and $\bar{X}_v = X_v$. When the circular current limiter is triggered, σ will decrease according to (3). A larger virtual impedance is thus introduced to limit the converter-side current, whose exact value is uniquely determined by the designed constant X/R ratio $\bar{X}_v/\bar{R}_v = X_v/R_v$ and the operating condition $\|i_{f\alpha\beta}\| = I_M$, i.e.,

$$\left\| \frac{\left(\frac{R_g + jX_g}{jX_c} + 1\right)\bar{V}^{\text{ref}} e^{j\delta} - V_g}{(\bar{R}_v + j\bar{X}_v)\left(\frac{R_g + jX_g}{jX_c} + 1\right) + R_g + jX_g} \right\| = I_M \tag{5}$$

where $X_g = \omega_g L_g$; $X_c = -1/\omega_g C_f$; V_g is the magnitude of the grid voltage; $\delta \triangleq \langle v_{\alpha\beta}^{\text{ref}}, v_{g\alpha\beta} \rangle$ is the angle difference between the voltage reference $v_{\alpha\beta}^{\text{ref}}$ and $v_{g\alpha\beta}$. It should be noted that the solutions $\bar{X}_v$ and $\bar{R}_v$ are functions of δ and $\bar{V}^{\text{ref}}$.

B. Closed-Loop System Dynamics

Based on the proposed equivalent circuit model, the closed-loop system dynamics can be expressed as

$$\begin{cases} \dot{\delta} = \dot{\theta}^{\text{ref}} - \omega_g = K_P^P (P^{\text{ref}} - P) \\ \dot{V}^{\text{ref}} = K_P^V (V^{\text{ref}} - \|v_{\alpha\beta}\|) \end{cases} . \tag{6}$$

As illustrated in Section III-A, $\bar{R}_v$ and $\bar{X}_v$ are two functions of δ and $\bar{V}^{\text{ref}}$. Therefore, the active power output P and $\|v_{\alpha\beta}\|$ are also two nonlinear functions of δ and $\bar{V}^{\text{ref}}$ whose detailed expressions can be obtained through $P = \text{Re}\{v_{\alpha\beta} i_{\alpha\beta}^*\}$ and the Kirchhoff's circuit laws.

IV. IMPACT OF CIRCULAR LIMITER ON TRANSIENT STABILITY

In this section, a time-rescaling technique is first utilized to reduce the number of control parameters required to be analyzed. Afterward, the phase plane analysis is applied to evaluate the impact of the circular current limiter on transient stability.

TABLE I.   SYSTEM AND CONTROL PARAMETERS

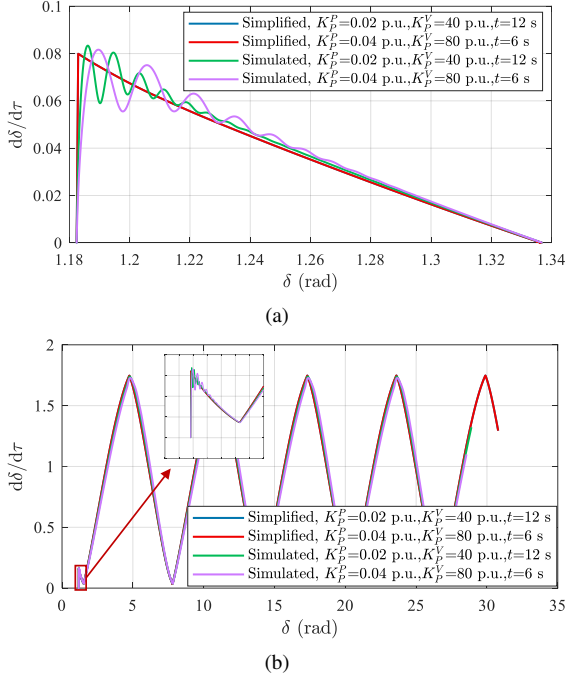| Quantity	Value
Grid phase voltage V_g	$55\sqrt{2}$ V (1 p.u.)
Grid angular frequency ω_g	100π rad/s (1 p.u.)
Grid impedance L_g and R_g	22 mH (0.952 p.u.), 0.3 Ω (0.041 p.u.)
LC-filter L_f and C_f	2 mH, 15 μF
Active power reference P^{ref}	1125 W (0.9 p.u.)
Voltage reference V^{ref}	1 p.u.
Maximum current I_M	1.2 p.u.
Virtual impedance L_v and R_v	0.3 p.u., 0.1 p.u.
Current control P & R gain	0.5 p.u., 50 p.u.
Current cotnrol ω_c	0.02 p.u.

(a)

(b)

Fig. 3.   Comparison between the proposed model (7) and the simulated result: (a) phase portraits under grid voltage drops 0.1 p.u.; (b) phase portraits under grid voltage drops 0.2 p.u.

A. Time-Rescaling Technique

Notice that there are two control parameters in the closed-loop system dynamics (6), i.e., K_P^P and K_P^V. To simplify the following transient stability analysis, a time-rescaling technique is introduced firstly. Define $\tau = K_P^P t$ as the scaled time. Based on the chain rule, (6) becomes

$$\begin{cases} \dfrac{\mathrm{d}\delta}{\mathrm{d}\tau} = P^{\text{ref}} - P \\ \dfrac{\mathrm{d}\bar{V}^{\text{ref}}}{\mathrm{d}\tau} = \dfrac{K_P^V}{K_P^P}(V^{\text{ref}} - \|v_{\alpha\beta}\|) \end{cases} . \qquad (7)$$

Hence, it can be observed that the closed-loop system dynamics is determined by only one control parameter K_P^V/K_P^P, which is defined as the "relative speed" between the voltage magnitude control loop and the power one.

With the system parameters in Table I, Fig. 3 gives two examples to illustrate the time-rescaling technique with two different parameters sets. In Fig. 3(a), both the simplified and simulated phase portraits under a grid voltage drop of 0.1 p.u. are given. One can see that these four phase portraits are
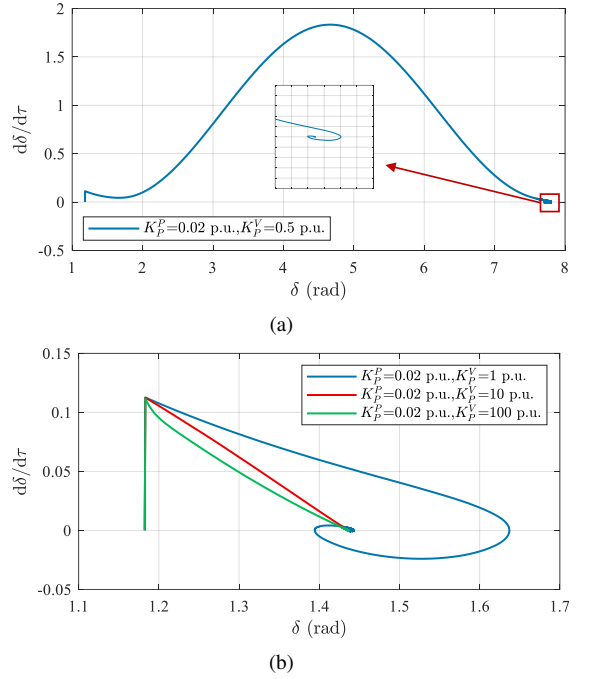

(a)

(b)

Fig. 4.   Phase portraits under a grid voltage drop (0.14 p.u.) w/o the circular limiter: (a) $K_P^V = 0.5$ p.u.; (b) K_P^V increases from 1 p.u. to 100 p.u.

close to each other since the relative speed K_P^V/K_P^P is fixed. The initial oscillations in the simulated phase portraits are introduced by the dynamics of the current control loop, the capacitor, and the inductors.

Next, Fig. 3(b) gives the phase portraits under a grid voltage drop of 0.2 p.u. Again, the results verify the effectiveness of the proposed time-rescaling technique and the accuracy of the proposed dynamic model.

B. Transient Stability Analysis

In the following analysis, the parameters in Table I are used. The transient stability of the GFM converter is investigated based on the phase plane analysis under an ultra-weak grid condition (SCR≈1.05). Based on the simplified model in (7), the power control gain K_P^P can be fixed and only the voltage magnitude control gain K_P^V is increased gradually for the transient stability analysis. A grid voltage drop of 0.14 p.u. is selected to ensure the existence of stable equilibrium points. The results are illustrated in Figs. 4-5.

When the circular current limiter is transparent, from the results in Fig. 4, one can notice that the transient stability of the GFM converter is ensured for a wide range of K_P^V, i.e., from 0.5 p.u. to 100 p.u. When $K_P^V = 0.5$ p.u., transient stability is ensured after one cycle of oscillation as shown in Fig. 4(a). From Fig. 4(b), it can be observed that the increase of the relative speed K_P^V/K_P^P is beneficial to transient stability.

When the circular current limiter is applied, the results are illustrated in Fig. 5. From Fig. 5(a) and 5(b), one can notice that transient stability is jeopardized when $K_P^V \leq 1$ p.u. and reacquired when K_P^V increases to 3 p.u. as shown in Fig. 5(b).
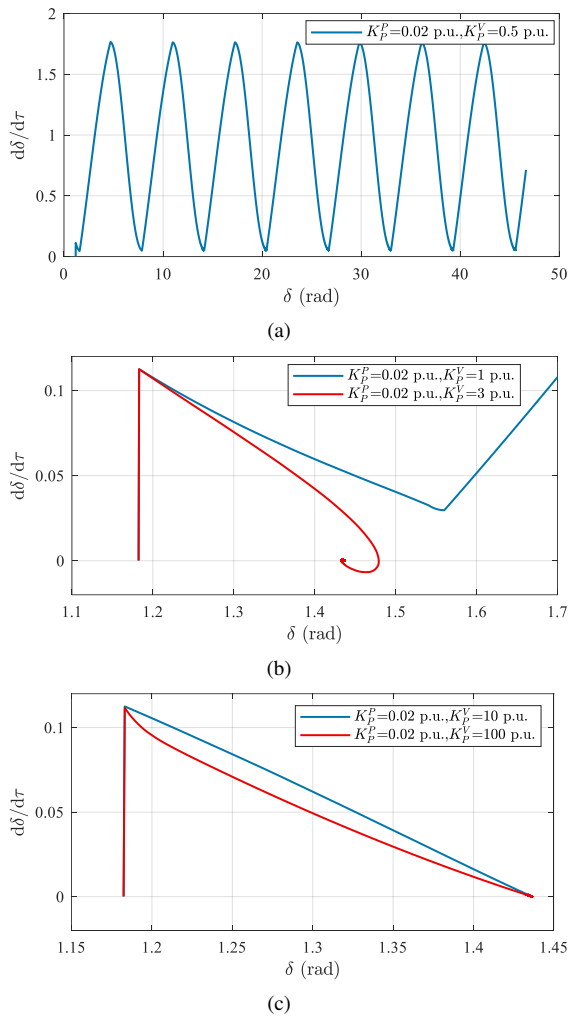
Fig. 5. Phase portraits under a grid voltage drop (0.14 p.u.) w/ the circular limiter: (a) $K_P^V = 0.5$ p.u.; (b) K_P^V increases from 1 p.u. to 3 p.u.; (c) K_P^V increases from 10 p.u. to 100 p.u.

Further, Fig. 5(c) shows that transient stability is ensured when K_P^V/K_P^P increases.

From the phase portraits in Figs. 4 and 5, it is revealed that the transient stability of a virtual-admittance-controlled GFM converter with a circular current limiter can be jeopardized when the relative speed K_P^V/K_P^P is small.

V. VERIFICATION STUDIES

A. Simulation Results

In this test, a grid voltage drop of 0.14 p.u. at 2 s is simulated to verify the transient stability analysis results. The system parameters in Table I are again applied. The power control gain is selected as $K_P^P = 0.02$ p.u. The corresponding system responses with different voltage magnitude control parameters are given in Figs. 6-7.

The results with $K_P^V = 1$ p.u. are given in Fig. 6. When the converter-side current is not constrained, transient stability is ensured when grid voltage drops. As shown in Fig. 6(a),
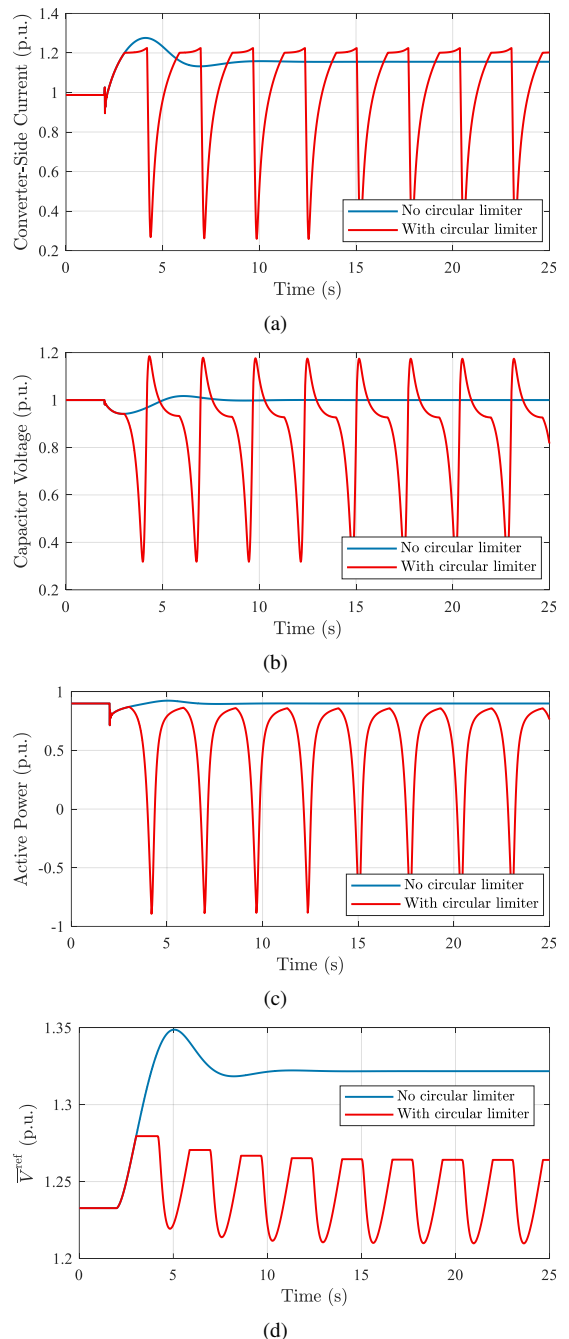
Fig. 6. System responses under grid voltage drops 0.14 p.u. with $K_P^P = 0.02$ p.u. and $K_P^V = 1$ p.u.: (a) converter-side current; (b) capacitor voltage; (c) active power; (d) $\bar{V}^{\text{ref}}$.

the converter-side current can exceed its maximum allowed value, i.e., 1.2 p.u., during the transient state. But it will finally converge to a steady-state value below 1.2 p.u. In comparison, when the circular current limiter is utilized, the transient stability of the GFM converter is jeopardized. From Figs. 6(b) and 6(c), periodic oscillations are observed in the capacitor voltage and active power output. From the trajectories of $\|i_{f\alpha\beta}\|$ and $\bar{V}^{\text{ref}}$ in Figs. 6(a) and 6(d), one can observe that the reason for this instability phenomenon is that $\bar{V}^{\text{ref}}$ fails to converge to its stable equilibrium point before the triggering
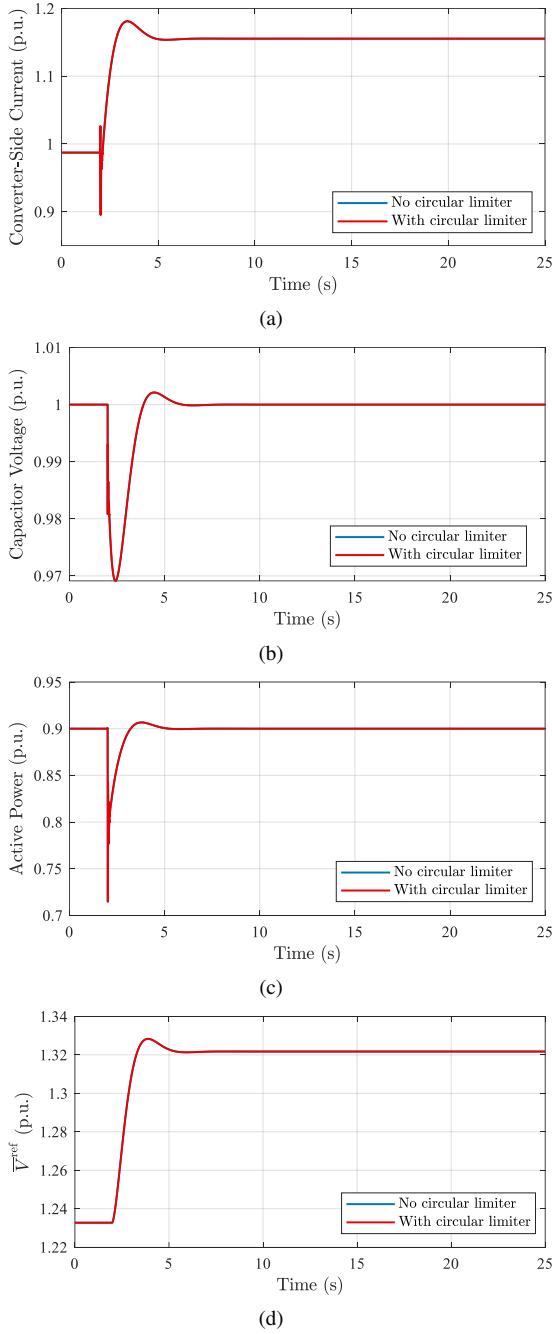
Fig. 7. System responses under grid voltage drops 0.14 p.u. with $K_P^P = 0.02$ p.u. and $K_P^V = 3$ p.u.: (a) converter-side current; (b) capacitor voltage; (c) active power; (d) $\bar{V}^{\text{ref}}$.

of the circular limiter. Consequently, the maximum value of $\bar{V}^{\text{ref}}$ decreases intermittently, and finally, the GFM converter loses an equilibrium point and fails to synchronize with the power grid.

Next, the control gain K_P^V is increased to 3 p.u. The corresponding results are given in Fig. 7. One can notice that the transient stability of the GFM converter is ensured with or without the use of the circular current limiter. From Figs. 7(a) and 7(d), $\bar{V}^{\text{ref}}$ can quickly converge to its equilibrium point
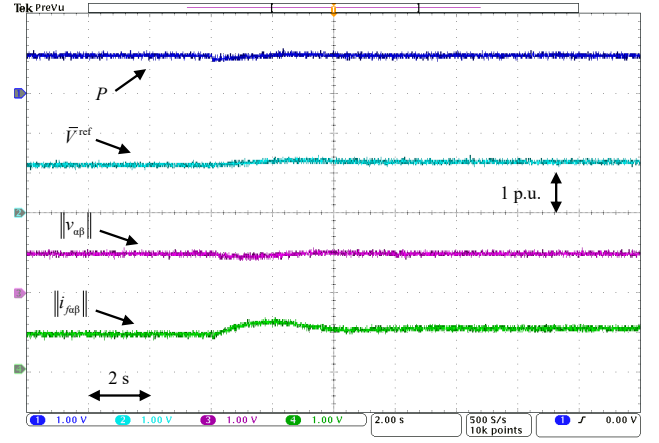

Fig. 8. Experimental results of under grid voltage drops 0.14 p.u. with $K_P^P = 0.02$ p.u. and $K_P^V = 1$ p.u. No circular current limiter is utilized.
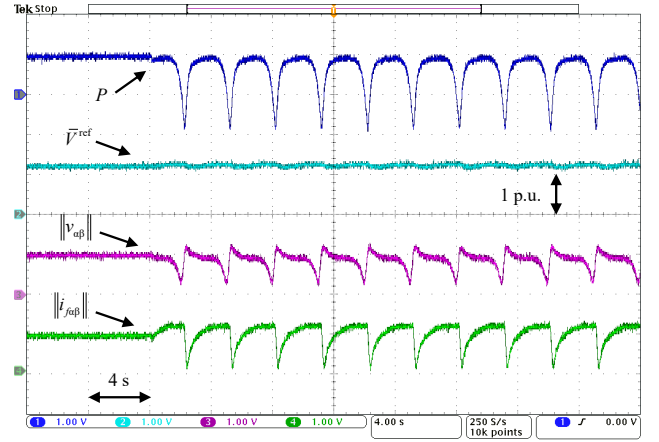

Fig. 9. Experimental results of under grid voltage drops 0.14 p.u. with $K_P^P = 0.02$ p.u. and $K_P^V = 1$ p.u. The circular current limiter is utilized.

without triggering the current limiter in the transient state. Therefore, transient stability is ensured. In addition, the system responses are identical in both cases since the converter-side current is always below 1.2 p.u. as demonstrated in Fig. 7(a).

B. Experimental Results

The stability analysis results are further verified on a prototype experimental setup, whose topology and parameters are discussed in [11]. In the experimental tests, the system and control parameters in Table I are used. The power control gain is again chosen as $K_P^P = 0.02$ p.u. A grid voltage drop of 0.14 p.u. is applied in these tests. The corresponding results are delivered in Figs. 8-11.

In Figs. 8-9, the voltage magnitude control parameter is selected as $K_P^V = 1$ p.u. When the circular current limiter is transparent, from Fig. 8, one can see that transient stability is ensured when the grid voltage drops to 0.86 p.u. The variable $\bar{V}^{\text{ref}}$ can converge to its equilibrium point finally, which is around 1.3 p.u. However, since no current limiter is used in this case, the converter-side current can temporarily exceed its
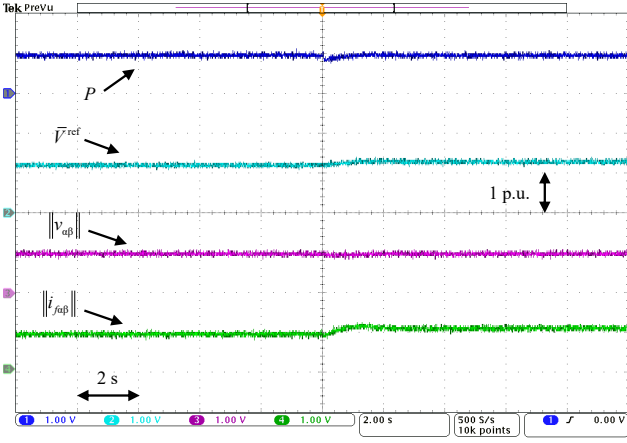
Fig. 10. Experimental results of under grid voltage drops 0.14 p.u. with $K_P^P = 0.02$ p.u. and $K_P^V = 3$ p.u. No circular current limiter is utilized.
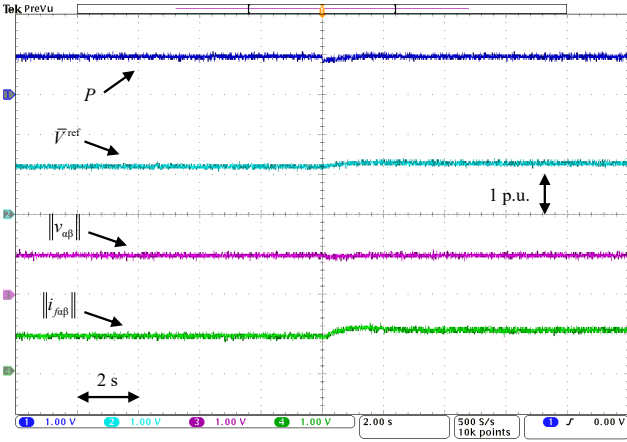

Fig. 11. Experimental results of under grid voltage drops 0.14 p.u. with $K_P^P = 0.02$ p.u. and $K_P^V = 3$ p.u. The circular current limiter is utilized.

maximum allowed value 1.2 p.u. In Fig. 9, the circular current limiter is applied. One can notice that V^{ref} fluctuates around 1.2 p.u., which is always smaller than its equilibrium point depcited in Fig. 8. Although the current limitation is achieved, the GFM converter becomes unstable.

Figs. 10-11 give the experimental results with the increased voltage magnitude control gain $K_P^V = 3$ p.u. Again, when the circular current limiter is transparent, transient stability is ensured under the grid voltage disturbance as shown in Fig. 10. The converter-side current is always below 1.2 p.u. When the circular current is applied, unlike the previous unstable results with $K_P^V = 1$ p.u., the GFM converter is still stable due to the quick adjustment of $\bar{V}^{\text{ref}}$ as shown in Fig. 11.

VI. CONCLUSION

In this study, the impact of the circular current limiter on the transient stability of a virtual-admittance-controlled GFM converter is investigated. It is found that for the transient stability analysis, the inner control loops with the circular limiter can be simplified as a voltage source behind adaptive virtual impedance. Based on a time-rescaling technique and the phase plane analysis, it is revealed that transient stability is only affected by the "relative speed" between the voltage magnitude control loop and the power one. Moreover, when the circular current limiter is applied, the transient stability of the GFM converter can be jeopardized, while reacquired by increasing the relative speed. Finally, these findings are verified by both simulation and experimental results.

REFERENCES

[1] T. Liu and X. Wang, "Transient stability of single-loop voltage-magnitude controlled grid-forming converters," *IEEE Trans. Power Electron.*, vol. 36, no. 6, pp. 6158–6162, 2020.

[2] R. Rosso, X. Wang, M. Liserre, X. Lu, and S. Engelken, "Grid-forming converters: Control approaches, grid-synchronization, and future trends-a review," *IEEE Open J. Ind. Appl.*, vol. 2, pp. 93–109, 2021.

[3] T. Qoria, F. Gruson, F. Colas, X. Kestelyn, and X. Guillaud, "Current limiting algorithms and transient stability analysis of grid-forming VSCs," *Elect. Power Syst. Res.*, vol. 189, p. 106726, 2020.

[4] R. Rosso, S. Engelken, and M. Liserre, "On the implementation of an FRT strategy for grid-forming converters under symmetrical and asymmetrical grid faults," *IEEE Trans. Ind. Appl.*, vol. 57, no. 5, pp. 4385–4397, 2021.

[5] T. Qoria, F. Gruson, F. Colas, G. Denis, T. Prevost, and X. Guillaud, "Critical clearing time determination and enhancement of grid-forming converters embedding virtual impedance as current limitation algorithm," *IEEE J. Emerg. Sel. Topics Power Electron.*, vol. 8, no. 2, pp. 1050–1061, 2020.

[6] L. Huang, H. Xin, Z. Wang, L. Zhang, K. Wu, and J. Hu, "Transient stability analysis and control design of droop-controlled voltage source converters considering current limitation," *IEEE Trans. Smart Grid*, vol. 10, no. 1, pp. 578–591, 2019.

[7] E. Rokrok, T. Qoria, A. Bruyere, B. Francois, and X. Guillaud, "Transient stability assessment and enhancement of grid-forming converters embedding current reference saturation as current limiting strategy," *IEEE Trans. Power Syst.*, early access, Aug. 26, 2021, doi: 10.1109/TP-WRS.2021.3107959.

[8] M. Awal and I. Husain, "Transient stability assessment for current constrained and unconstrained fault ride-through in virtual oscillator controlled converters," *IEEE J. Emerg. Sel. Topics Power Electron.*, early access, May 13, 2021, doi: 10.1109/JESTPE.2021.3080236.

[9] X. Wang, M. G. Taul, H. Wu, Y. Liao, F. Blaabjerg, and L. Harnefors, "Grid-synchronization stability of converter-based resources–an overview," *IEEE Open J. Ind. Appl.*, vol. 1, pp. 115–134, 2020.

[10] M. G. Taul, X. Wang, P. Davari, and F. Blaabjerg, "Current limiting control with enhanced dynamics of grid-forming converters during fault conditions," *IEEE J. Emerg. Sel. Topics Power Electron.*, vol. 8, no. 2, pp. 1062–1073, 2020.

[11] B. Fan and X. Wang, "A Lyapunov-based nonlinear power control algorithm for grid-connected VSCs," *IEEE Trans. Ind. Electron.*, early access, Mar. 17, 2021, doi: 10.1109/TIE.2021.3065614.